Research Article

Amirhosein Fathi, Farzad Kermani, Aliasghar Behnamghader, Sara Banijamali, Masoud Mozafari*, Francesco Baino, and Saeid Kargozar*

Three-dimensionally printed polycaprolactone/multicomponent bioactive glass scaffolds for potential application in bone tissue engineering

Abstract: Over the last years, three-dimensional (3D) printing has been successfully applied to produce suitable substitutes for treating bone defects. In this work, 3D printed composite scaffolds of polycaprolactone (PCL) and strontium (Sr)- and cobalt (Co)-doped multi-component melt-derived bioactive glasses (BGs) were prepared for bone tissue engineering strategies. For this purpose, 30% of as-prepared BG particles (size <38 μm) were incorporated into PCL, and then the obtained composite mix was introduced into a 3D printing machine to fabricate layer-by-layer porous structures with the size of $12 \times 12 \times 2$ mm^3.

The scaffolds were fully characterized through a series of physico-chemical and biological assays. Adding the BGs to PCL led to an improvement in the compressive strength of the fabricated scaffolds and increased their hydrophilicity. Furthermore, the PCL/BG scaffolds showed apatite-forming ability (*i.e.*, bioactivity behavior) after being immersed in simulated body fluid (SBF). The in vitro cellular examinations revealed the cytocompatibility of the scaffolds and confirmed them as suitable substrates for the adhesion and proliferation of MG-63 osteosarcoma cells. In conclusion, 3D printed composite scaffolds made of PCL and Sr- and Co-doped BGs might be potentially-beneficial bone replacements, and the achieved results motivate further research on these materials.

Keywords: three-dimensional (3D) printing, composite scaffolds, bioactive glass, polycaprolactone, bone tissue engineering

Corresponding Author: Masoud Mozafari: Department of Tissue Engineering & Regenerative Medicine, Faculty of Advanced Technologies in Medicine, Iran University of Medical Sciences, Tehran, Iran; Lunenfeld-Tanenbaum Research Institute, Mount Sinai Hospital, University of Toronto, Toronto, ON, Canada; Email: Mozafari.masoud@gmail.com
Corresponding Author: Saeid Kargozar: Tissue Engineering Research Group (TERG), Department of Anatomy and Cell Biology, School of Medicine, Mashhad University of Medical Sciences, Mashhad 917794-8564, Iran; Email: Kargozarsaeid@gmail.com
Amirhosein Fathi: Bioengineering Research Group, Nanotechnology and Advanced Materials Department, Materials and Energy Research Center (MERC), Alborz, Iran
Farzad Kermani: Department of Materials Engineering, Faculty of Engineering, Ferdowsi University of Mashhad (FUM), Azadi Sq., Mashhad 917794-8564, Iran
Amirhosein Fathi and **Farzad Kermani** contributed equally to this work
Aliasghar Behnamghader: Biomaterials Research Group, Nanotechnology and Advanced Materials Department, Materials and Energy Research Center (MERC), Alborz, Iran
Sara Banijamali: Ceramic Department, Materials and Energy Research Center (MERC), Alborz, Iran
Francesco Baino: Institute of Materials Physics and Engineering, Applied Science and Technology Department, Politecnico di Torino, Corso Duca degli Abruzzi 24, 10129 Torino, Italy

1 Introduction

Treating and managing bone lesions (*e.g.*, fractures and tumors) are still among the most challenging issues in medicine [1]. The general increase of the elderly population combined with the high rate of chronic diseases, accidents, and obesity warn an urge for developing and utilizing more effective and efficient therapies for the replacement of injured and damaged tissues. Although auto-, allo-, and xenografts still are the first option in the operating rooms, drawbacks of transplant materials such as the limited harvesting tissue, the shortage of donors, and the risk of disease transmission are restricting their usage in the modern medicine era [2]. Therefore, synthetic biomaterials, including polymers as well as glass and glass-ceramics, have attracted much attention in bone tissue engineering (BTE) strategies.

Poly (ϵ-caprolactone) (PCL) is a biocompatible and biodegradable polymer that is considered as a long-term implant and drug delivery vehicle. However, the slow rate of degradation, poor mechanical properties, as well as hydrophobicity and consequent low cell adhesion limit the extensive usage of PCL in BTE [3, 4]. Although hydrophobic surfaces are mentioned as more suitable substrates for adsorbing greater amounts of proteins than neutrally charged hydrophilic surfaces, accelerated osteogenesis and increased bone-to-implant contact could be achieved by applying hydrophilic surfaces [5, 6]. The incorporation of bioactive glasses (BGs) into PCL has been suggested as a wise approach to improve surface hydrophilicity. BGs are highly versatile and useful materials in BTE applications since they possess excellent biocompatibility, osteoconductive and osteoinductive features, as well as the ability to bond to the living tissues [7, 8]. Prior studies have shown that adding BG particles to PCL could result in creating a class of composite scaffolds with significantly improved mechanical properties, tunable degradation rates, and increased bioactivity [9, 10]. Moreover, the introduction of BG microparticles into a PCL matrix results in an improvement in the hydrophilicity and subsequent better cell interactions [11]. In order to further improve the biological activity of BGs and their composites, innovative glass formulations are currently developed by incorporating metallic dopants with specific therapeutic properties [12]. In this regard, strontium- and cobalt-doped BGs were reported suitable materials in BTE application due to their ability to simultaneously accelerate osteogenesis and angiogenesis [13–15].

The use of novel technologies in BTE approaches is of great importance as three-dimensional (3D) printing by using computer-aided design (CAD) and computer-aided manufacturing (CAM) is considered a cutting-edge technique towards personalized medicine for bone tissue regeneration. The precise and controllable fabrication process of 3D printing may result in an artificial replacement mimicking the native structure and biological functions of the bone [16]. Up to now, a broad range of 3D printed constructs has been prepared and used for replacing various types of bone defects [17]. Since the bone tissue is actually a composite, the successful use of 3D printed polymer/glass composites was previously reported for BTE applications [18–21]. The formulation and composition of composite scaffolds may directly affect the final fate of a bone substitute *in vivo*; more research is still required to develop an optimal 3D printed scaffold for bone repair and regeneration.

In the present study, we could successfully prepare 3D printed scaffolds of PCL and Sr-/Co-doped BGs by using the FDM technique. The goal was to take benefit from using osteogenic and angiogenic BGs [22] to improve the cytocompatibility of PCL in the final 3D printed composite scaffolds. The fabrication of 3D printed PCL/BG composite scaffolds by robotic deposition has already been reported in the literature, but the BG compositions used were relatively simple, for example belonging to a SiO_2-CaO-P_2O_5 ternary system [23]. To the best of the authors' knowledge, the use of complex multi-component glass compositions (with 6 to 8 oxides) is reported here for the first time, along with the application of the FDM to process such materials.

2 Materials and methods

2.1 Glass synthesis

The synthesis of the BGs was described in a previous study [22]. Briefly, the BGs were synthesized in a multi-component system of $SiO_2-P_2O_5-CaO-SrO-CoO-Na_2O$-$MgO$-$K_2O$ by the melt–quench method. In order to obtain each BGs, appropriate amounts of oxides were melted in a platinum-rhodium crucible for 1.5 h at 1400°C in an electric furnace (Lenton, Hope Valley, UK). After this step, the glasses were rapidly quenched into the water to obtain a frit, and then the dried samples were ground using a vibratory puck mill (Gyro Mill, Glen Creston, London, UK) for 15 min and sieved to obtain the BG particles (d50 and d95 were 9.2 and 23.1 µm, respectively) to be then used for scaffold fabrication. Four different types of 3D printed scaffolds were fabricated in which Sr- and Co-doped BGs were incorporated into PCL substrates (see Table 1).

Table 1: Different formulations of the 3D printed composite scaffolds made of PCL containing 30% of Sr- and Co-doped BGs

Scaffold name	Glass composition (mol.%)							
	SiO_2	P_2O_5	CaO	SrO	Na_2O	MgO	K_2O	CoO
PCL/BG-Ca	41.2	5.06	36.14	0	7.17	3.26	7.17	0
PCL/BG-Sr	41.2	5.06	30.14	6	7.17	3.26	7.17	0
PCL/BG-CaCo	41.2	5.06	35.64	0	7.17	3.26	7.17	0.5
PCL/BG-SrCo	41.2	5.06	29.64	6	7.17	3.26	7.17	0.5
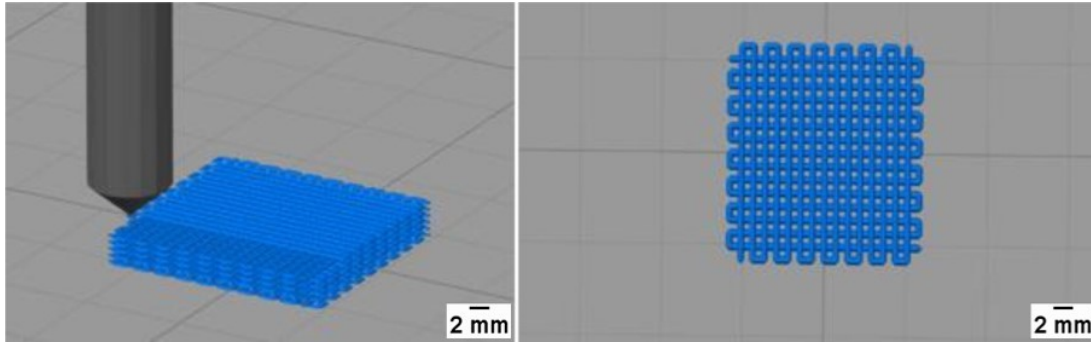
Figure 1: Schematic representation of side view (left) and top view (right) of the 3D printed slices by using Simplify3D software

2.2 Preparation of 3D printed scaffolds

In order to fabricate composite materials for scaffold production, 10 g of PCL (M_n = 80000 g/mol, d = 1.145 g/mL) was dissolved in 100 mL of chloroform ($CHCl_3$, M_w = 119.38, d = 1.48 g/mL) using a magnetic stirrer (Lab Tech, LMS 1003, South Korea) at 50°C and speed of 500 rpm for 1 h. Then, 3 g of the synthesized BGs was added to the solutions and stirred at 700 rpm until obtaining a viscous suspension. The resultant suspension was dried, and the obtained samples were then ground using a vibratory puck mill (Gyro Mill, Glen Creston, London, UK) for 15 min. The granules were finally used for the 3D printing process in five groups, namely PCL, PCL/BG-Ca, PCL/BG-Sr, PCL/BG-CaCo, and PCL/BG-SrCo.

3D porous cube-shaped structures were designed to have 30 % porosity, 12 mm in height, 12 mm in internal diameter with 2 mm wall thickness, raster angle of 0°-90°, and the spacing between the filaments of 400 µm using the Rhinoceros 5 3D CAD modeling package (3D CAD, Robert McNeel & Associates, USA). The Rhinoceros model was saved to stereolithography (STL) file and then converted into a g-code via Simplify3D software (Simplify3D, LLC, Ohio, USA) and imported into the 3D printing machine (3DPL Bioprinter N1, Iran). The granular substrates were melted in a heating jacket at 120°C, and the 3D scaffolds were deposited layer-by-layer using a nozzle size of 500 µm (see Figure 1).

2.3 Surface treatment of 3D printed scaffolds

The printed composite scaffolds were surface-treated to remove non-projected granules (the granules, which may have remained unchanged after the printing process) and improve the surface hydrophilicity. For this aim, three scaffolds of each group were soaked in a sodium hydroxide solution (NaOH, 5 M) at 37°C for 1 h. Then, the samples

were washed with deionized water three times. The surface wettability of scaffolds was estimated using contact dynamic angle analysis (CA-ES10, EOR Tech, Iran) according to standard ASTM D7334.

2.4 Physico-chemical characterization of scaffolds

2.4.1 Porosity measurements

The apparent porosity (πa) (%) and bulk density (ρ_b) (%) of the scaffolds were measured via immersing the samples in ethanol according to the Archimedes method (standard ISO 5017:2013):

$$\pi a = ((m_3 - m_1) / (m_3 - m_2)) \cdot 100 \tag{1}$$

$$\rho_b = (m_1 / (m_3 - m_2)) \cdot 100 \tag{2}$$

Where m_1 is the weight of the dry scaffold, m_2 is the weight of the immersed sample in water, and m_3 is the weight of the immersed sample in water and the suspended weight of the sample in water.

2.4.2 Compressive tests

The mechanical properties of the 3D printed scaffolds were evaluated under compressive load via a universal testing machine (Zwick Z005, Germany) with a 2.5 kN load cell and a crosshead speed of 1 mm/min. All scaffolds were loaded until 30% of strain. The compressive Young's modulus (E) of scaffolds was estimated by measuring the slope of the stress-strain curve in the linear elastic region. The tests were performed on three samples per each type; the results were expressed as mean ± standard deviation.

2.4.3 Structural characteristics

The phase composition of the 3D printed constructs was investigated using X-ray diffraction (XRD) analysis (D8-Advance Bruker, Germany) (step size 0.01°, time per step 1 s) before and after the incubation in simulated body fluid (SBF). The crystallinity of the newly-formed calcium phosphate phase grown on the scaffolds was estimated by using the relation proposed by Landi *et al.* [24]:

$$X_c \approx 1 - V_{112/300}/I_{300} \qquad (3)$$

where X_c is crystallinity degree, $V_{112/300}$ is the intensity of the hollow between (1 1 2) and (3 0 0) reflections, and I_{300} is the intensity of (3 0 0) reflection.

2.4.4 FTIR analysis

The inorganic bands of the fabricated scaffolds after the incubation in SBF were evaluated using Fourier transformed infrared spectroscopy (FTIR) (Thermo Nicolet AVATAR 370, USA) in the range of 400–4000 cm^{-1}. The bands were recognized using KBr pellets (1% wt/wt) when 64 scans were accumulated using a nominal resolution of 4 cm^{-1}.

2.4.5 Microscopic observations and compositional analysis

The surface morphology and the shape of the 3D printed scaffolds were observed using the field-emission scanning electron microscopy (FESEM) (MIRA3, TESCAN, CZ) before and after the immersion in SBF with an accelerated voltage of 20 kV. Compositional analysis was also performed by Energy-dispersive X-ray spectroscopy (EDX) and elemental mapping (the probe was included in the FESEM instrument).

2.4.6 *In vitro* bioactivity assessment

The SBF used in this study was prepared according to the Kokubo method [25]. In order to evaluate *in vitro* bioactivity, the scaffolds were immersed in SBF using a mass-to-liquid ratio of 1.5 mg/mL (as suggested in [26]) and were then placed in an orbital shaker (Thermo shake, Germany) with a speed of 20 rpm at the temperature of 37°C for the time periods of 1, 4, and 14 days. The pH of the media was controlled during the test by a universal digital pH meter (AZ pH Meter 86552, Taiwan). The weight changes of the scaffolds were also measured at the different time points (1, 4, and 14 days). The concentrations of Ca^{2+} and the released Sr^{2+} and Co^{2+} ions in the SBF were measured by using Atomic absorption spectroscopy analysis (AAS) in the incubation time periods mentioned above.

2.5 Evaluation of *in vitro* cellular behavior

2.5.1 Cell viability

The effect of the 3D printed scaffolds on the growth and proliferation of MG-63 osteosarcoma cells (National Cell Bank, Pasteur Institute of Iran) was determined via a standard colorimetric MTT ([3-(4,5-dimethyl-2-thiazolyl)-2,5-diphenyl tetrazolium bromide]) assay. For this purpose, 2.5×10^5 cells were seeded in 12-well plates (SPL Lifesciences, South Korea) and cultured with the RPMI-1640 supplemented by 10% fetal bovine serum (FBS) and 1% penicillin/streptomycin solution (Gibco, USA) in a humidified atmosphere of 5% CO$_2$ at 37°C. After 24 h of incubation, the scaffolds (1×1×1 mm^3) were UV-sterilized (60 min) and then added to the cell culture plates. The scaffolds were removed from the cell culture plate after an additional 24 h incubation, and the MTT solution (5 mg/mL) (Sigma-Aldrich, USA) was added to the cells and maintained in a humidified atmosphere of 5% CO$_2$ at 37°C for 4 h. After that, all the media were pulled out and dimethyl sulfoxide (DMSO) solution (Sigma-Aldrich, USA) was added to the plates and shaken for 10 min. The solutions were then transferred to 96-well cell culture plates to read the absorption of the samples by using Synergy H4 Hybrid Multi-Mode Microplate Reader (Synergy HT, BioTek, USA) at 570 nm. The experiments were conducted in triplicate, and all of the data were reported as mean ± standard deviation; cells in culture medium without scaffold were used as a control.

2.5.2 Cell attachment study

The morphology of adhered MG-63 cells onto the surface of the 3D scaffolds was investigated by field emission scanning electron microscopy (FESEM) analysis. First, each side of the 3D-scaffolds was sterilized for 30 min under the UV-irradiation. Then, the UV-sterilized 3D scaffolds were washed with phosphate-buffered saline (PBS) (Gibco, USA) three times, and 2.5×10^4 cells were seeded onto them. Then the samples were incubated for 3 days at 37°C in a humidified atmosphere of 5% CO$_2$. After the incubation time, the samples were placed into a solution containing 2.5% (v/v) glutaraldehyde (Merck, Germany) for 24 h, and the samples were then dehydrated in an increasing concen-

tration of ethanol for 30 min in each step (30%, 50%, 75%, and 100%). Finally, the samples were freeze-dried (BOC Edwards, Crawley, UK) for 24 h and sputter-coated (Edwards coating system E306A, UK) by gold for 10 min prior to being analyzed.

2.6 Statistical evaluations

The obtained results were statistically evaluated by using post hoc tests with two-way analysis of variance (ANOVA). The statistical analyses were conducted in triplicate, and all of the data were reported as mean ± standard deviation. Probability values less than 0.05 were considered significant (* $p < 0.05$, ** $p < 0.01$, *** $p < 0.001$, and **** $p < 0.0001$) (GraphPad Prism, San Diego, CA, USA).

3 Results and discussion

3.1 Surface wettability

The surface hydrophilicity of scaffolds is beneficial in the interaction with the biological environment and would affect cell adhesion and cell growth [27]. The contact angle analysis results (see Figure S1) show the surface wettability of the composite scaffolds. According to the data, the hydrophilicity of the PCL/BG-SrCo with an average contact angle of 76°C is higher than PCL with an average contact angle of 96.6°C, which indeed suggested an improvement of hydrophilicity in PCL/BG scaffolds. The observed increase in hydrophilicity of PCL/BG scaffolds compared to PCL is attributed to the obvious presence of glass particles; in this regard, it was suggested that the higher roughness of PCL/BG composites compared to the polymer alone may play a role [28]. Moreover, the NaOH surface treatment further improved the hydrophilicity of scaffolds. After treatment with NaOH, the contact angle of PCL and PCL/BG-SrCo decreased to 76°C and 61.6°C, respectively. Also in this case, an increase in the hydrophilicity of the scaffolds was suggested to be associated with an increase in the surface roughness of scaffolds After NaOH treatment [20].

3.2 Morphology

The apparent porosity of the 3D printed composite scaffolds was about 25%, which is indeed below the designed porosity (30 %) (See Table 2). The difference between the value of apparent porosity and designed porosity may be related to the footprint phenome in the 3D printing process [29, 30]. The bulk density of the scaffolds is higher than 80% (See Table 2), which implies the usefulness of the scaffolds in the case of BTE applications [31, 32].
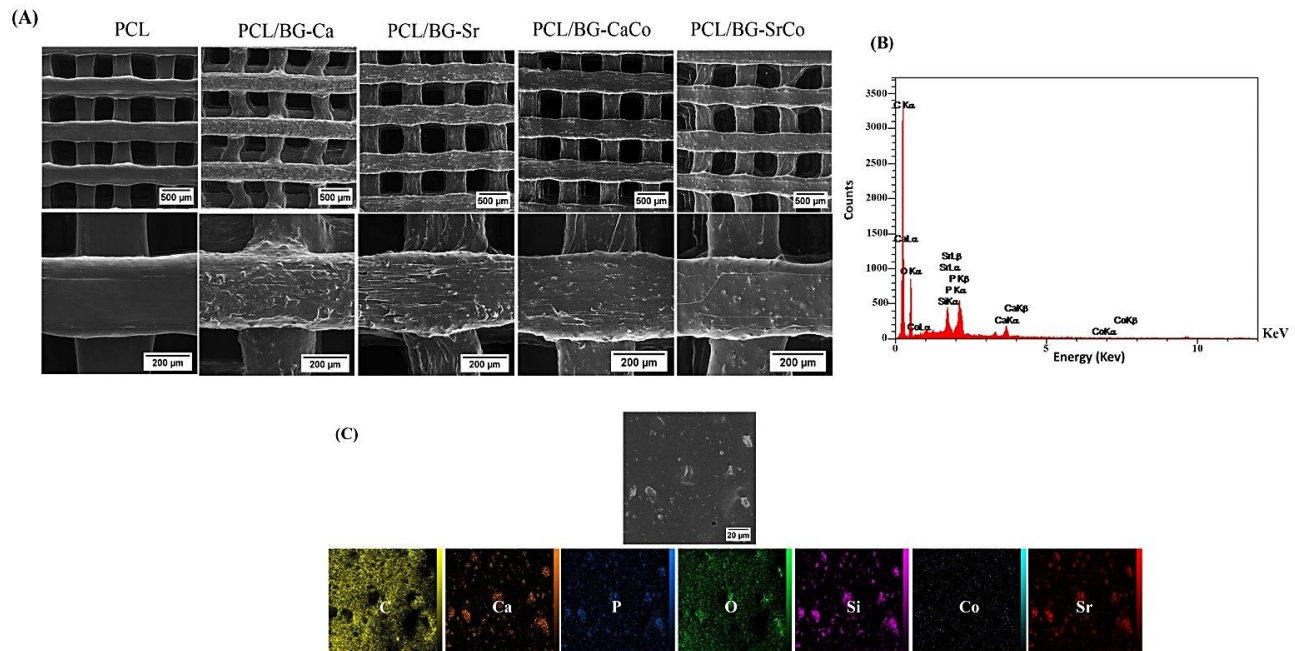
Figure 2: A) The SEM images of the 3D printed scaffolds exhibiting their surface morphology; B) Energy-dispersive X-ray spectroscopy (EDX) of the PCL/ BG-SrCo composite scaffold; C) Elemental mapping of the PCL/BG-SrCo scaffolds

Table 2: Calculation of the porosity of scaffolds via the Archimedes method

	PCL	PCL/BG-Ca	PCL/BG-Sr	PCL/BG-CaCo	PCL/BG-SrCo
πa (%)	26.8 ± 1.1	25.8 ± 1.2	26.3 ± 0.9	26.0 ± 1.4	25.9 ± 1.3
ρ_b (%)	80.9	81.8	81.3	81.6	81.7

Figure 2A shows the FESEM micrographs of the 3D printed PCL and PCL/BG composite scaffolds. Based on the presented data, the surface roughness of PCL/BG increased compared to the printed PCL due to the presence of glass inclusions protruding from the polymer. The scaffold structure fixed at the design stage (CAD file) is well reproduced in the final product. The presence of an ordered arrangement of parallel macro-channels (lumen about 400 µm) will be key to allow biological fluids to flow in/out the scaffolds, cells to colonize the whole scaffold volume, and newly-formed tissue to grow in vivo [33]. Figure 2B shows the EDX analysis of PCL/BG-SrCo composite scaffolds. According to EDX analysis, the C, Si, Ca, P, O, Sr, and Co ions were detected. Figure 2C shows the elemental mapping analysis of the PCL/BG-SrCo scaffolds. The dispersion of BGs in the PCL matrix is acceptable according to the elemental mapping plots. Using FDM to print the PCL/BG scaffolds carries an important advantage, as the structural control of 3D scaffolds obtained from polymeric pastes dissolved in solvents – which is needed in other additive manufacturing technologies – is generally difficult due to the challenge of controlling the fate of the solvent. In fact, as pointed out by Yun *et al.* [23], the uncontrolled elimination of solvent could lead to unpredictable shrinkage, and/or the solvent remaining in the extruded polymer-based filament may cause the extruded struts to fuse together, thereby inducing the collapse of the 3D architecture.

3.3 Structural characteristics

The XRD results of the 3D printed scaffolds are presented in Figure 3. The results indicated the semi-crystalline structure of the printed PCL. As revealed in Figure 3, the PCL has two main peaks at 2θ about 21.3° and 23.6°, which correspond, respectively, to the (110) and (200) reflections of the orthorhombic structure. These results are in good agreement with the crystallization behaviors reported for PCL networks [34], PCL/carbon nanotubes composites [35], and PCL/polyethylene glycol coatings [36]. Some minor peaks, located at 19.3° and 29.7°, are also observed, which are related to the polymer chains generated in chloroform evaporation and printing process [37, 38]. The XRD results of printed PCL/BG composite scaffolds demonstrated a lit-
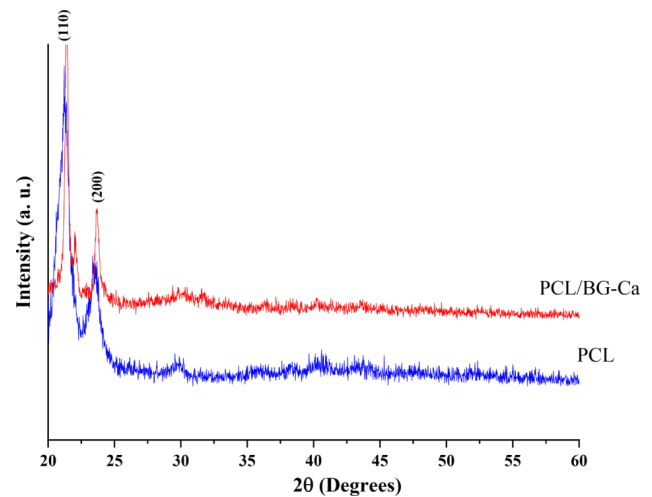
Figure 3: The XRD data of the PCL and PCL/BG-Ca scaffolds before immersing in SBF

tle shift to higher 2θ values and an increased intensity of the peak around 22.1°. These changes are due to the difference in the coordination of PCL molecules in the PCL/BG composite scaffolds, as suggested elsewhere [39]. No diffraction peak could be associated with the presence of glasses, which remained amorphous during the printing process.

3.4 Mechanical properties

The strain-stress curves of the 3D printed PCL, PCL/BG-Ca, PCL/BG-SrCo composite scaffolds are illustrated in Figure 4. According to the data, the estimated compressive Young's modulus of PCL, PCL/BG-Ca, PCL/ BG-SrCo are 7.5 ± 0.9, 8.7 ± 0.9, and 9.3 ± 0.7 MPa, respectively. The presence of stiff inclusions of glass within the polymeric matrix leads to an increase of Young's modulus, which is in agreement with previously reported studies [40]. It is interesting to observe that the values of Young's modulus are 2 to 4 times higher than that reported by Yun *et al.* [23] for robocasting PCL/BG scaffolds. The reason may be connected with the higher porosity (>70%) of Yun's samples due to the incorporation of mesoporous bioactive glass (MBG). The reason behind the difference between the Young compressive modulus of the PCL/BG-Ca and PCL/ BG-SrCo may be related to the expansion of the glass network when strontium and cobalt

are substituted with calcium ions [40]. However, the mechanical properties, *i.e.*, Young's modulus, of the PCL/BGs scaffolds with a porosity of 60% was previously reported

in higher amounts (90 MPa), which may be related to the higher content of glass particles in the composites (50 wt.%) as well as the different applied method (the supercritical CO_2 approach) [41].
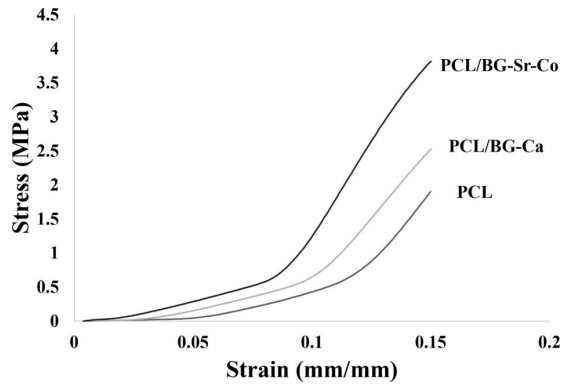
Figure 4: The stress-strain of the PCL, PCL/BG-Ca, and PCL/BG-SrCo scaffolds

3.5 Surface morphology and *in vitro* bioactivity assessments

The *in vitro* bioactivity results of the prepared scaffolds are illustrated in Figure 5. FESEM images (Figure 5A) reveal the formation of globular agglomerates on the surface of the scaffolds after 14 days of incubation in SBF. This newly-formed phase exhibits a cauliflower morphology that is very similar to that of the typical hydroxycarbonate apatite (HCA)-like layer detected on the surface of silicate BGs upon this kind of test. The EDX analysis of this layer formed on the PCL/BG-SrCo scaffolds was presented in Figure 5B. The
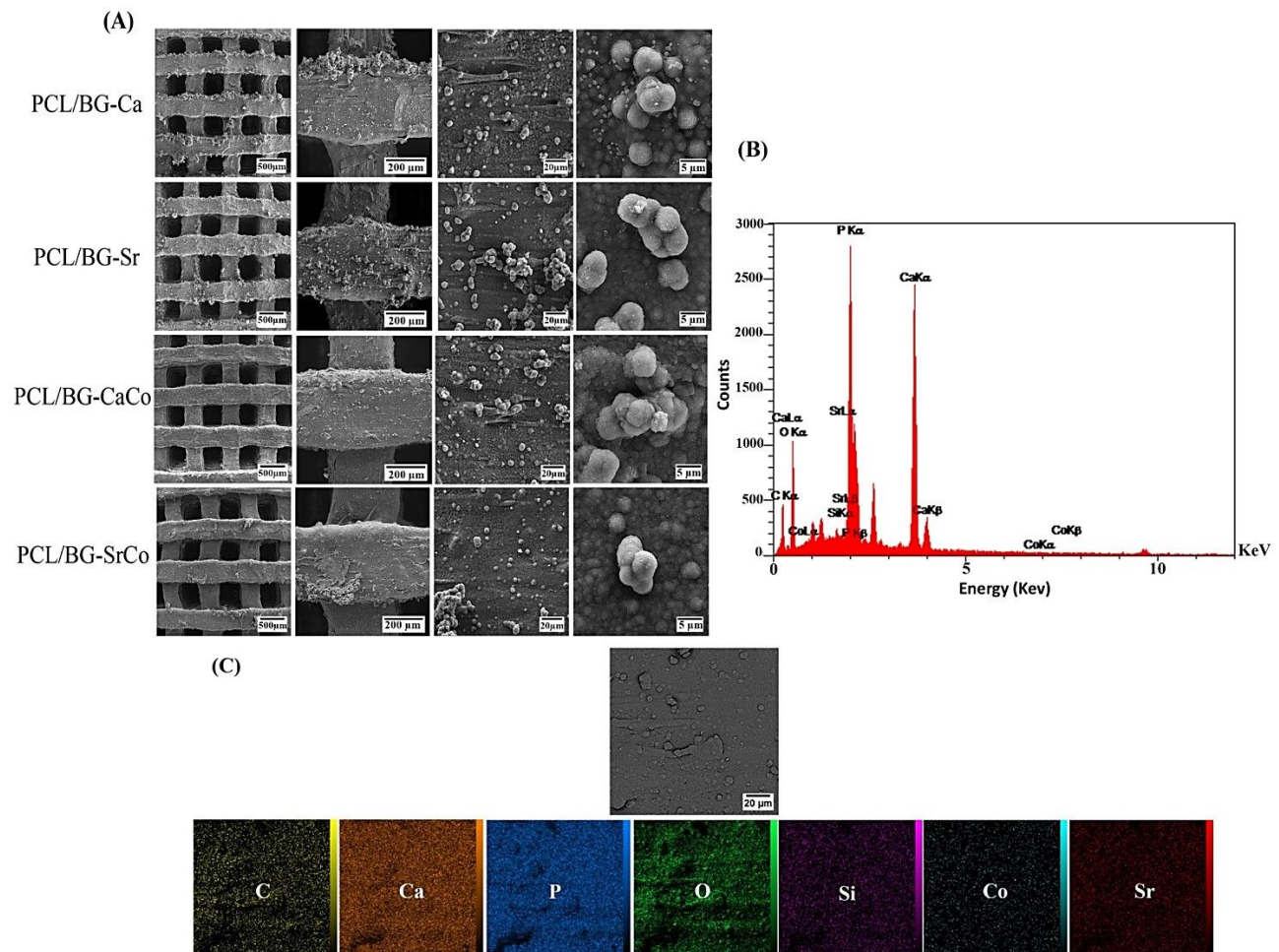
Figure 5: A) SEM micrographs of the printed composite scaffolds after 14 days of the immersion in SBF; B) The EDX analysis of the 3D printed scaffolds showing the newly formed HAp like layer on their surface post 14 days of incubation; C) Elemental mapping of the newly formed layer on the surface of 3D printed scaffolds after 14 days of incubation
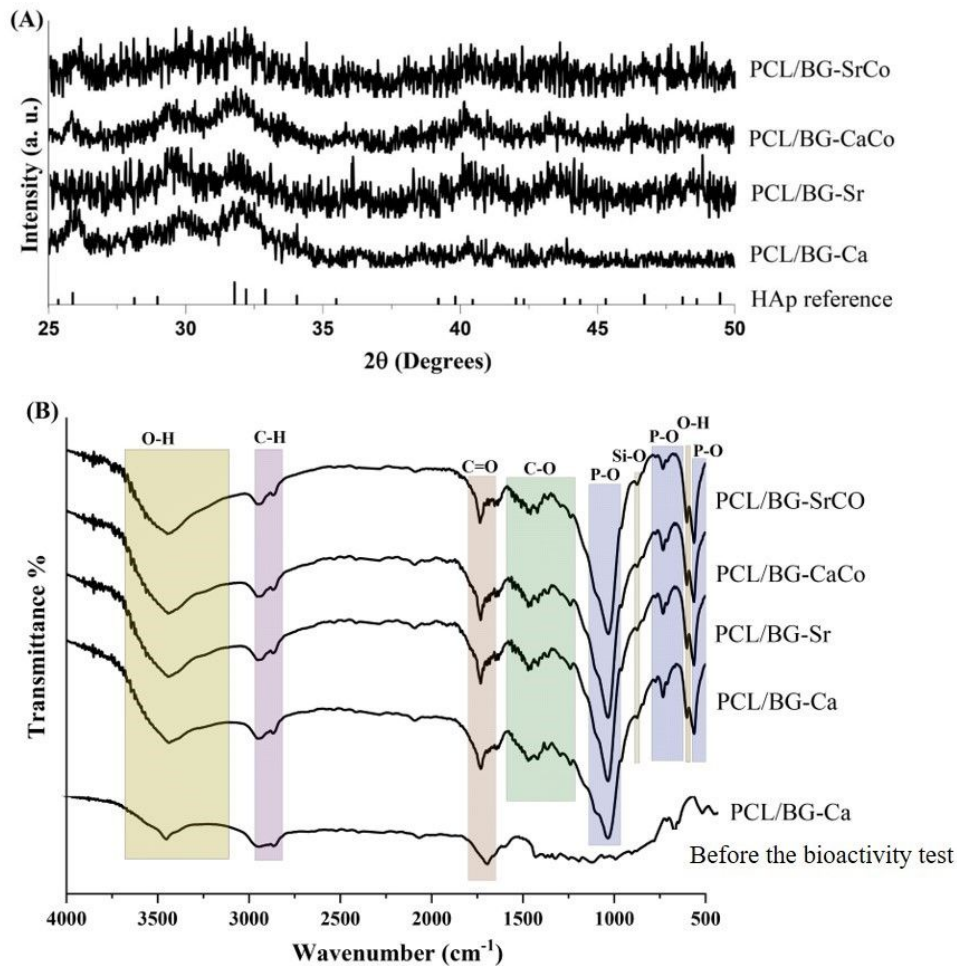
Figure 6: A) The XRD diffractogram of the 3D printed scaffolds clarifying the newly formed HAp like layer on their surface after 14-days of incubation in SBF; B) The FTIR spectra of different 3D printed scaffolds exhibiting the newly formed layer on their surface after 14 days of incubation

EDX analysis detected the presence of most elements contained in the glass oxides (Si, Ca, P, Sr, and Co), but it is evident the high intensity of the peaks associated with Ca and P, the abundance of which increased on the surface of the SBF-incubated samples as compared to their counterparts before the immersion in SBF (Figure 2B). Elemental mapping (see Figure 5C) confirmed the prevalence of Ca, P, O, and C on the surface of the incubated BG as well as the homogenous mineralization of the HCA layer that covers the glass lying underneath.

The nature of this newly-formed CaP phase was determined by using XRD and FTIR analysis. According to XRD diffractograms (Figure 6A), the hydroxyapatite (HAp, Reference code: 00-009-0432, $(Ca_{10}(PO_4)_6(OH)_2)$, Hexagonal, $P6_3m/173$)) the phase was detected on the surface of the scaffolds. Specifically, the samples exhibited the characteristic (0 0 2) and (2 1 1) reflections for HAp at 2θ = 26.4 and 32,3°; the peaks are broad due to the nano-crystalline

nature of this phase. The calculations of the crystallinity (Table 3) showed the crystallinity degree of the HAp phase on the surface of the scaffold, which is within 19-24%. The highest crystallinity of HAp (24%), associating with a higher rate of the bioactive process [42], belongs to the PCL/BG-Sr-Co group. The higher bioactivity of multi-doped BG-Sr-Co is justified due to higher amounts of structural defects, especially oxygen vacancies in the multi-doped glass structure [43].

Table 3: The crystallinity of the formed HAp layer after 14 days

Sample	Crystallinity of HAp phase (%)
PCL/BG-Ca	19.13
PCL/BG-Sr	18.40
PCL/BG-CaCo	18.24
PCL/BG-SrCo	23.87

FTIR spectra of the scaffolds incubated in SBF (14 days) are depicted in Figure 6B. The bands in the range of (560–630) and (1000–1100) cm^{-1} are related to P-O bonds, which are attributed to the presence of the HAp phase [7]. Besides, the band for O-H bonds, which was observed around 630 cm^{-1}, is attributed to structural groups of HAp, as well [44]. The observed broad C-O band in the range of (1460–1560) cm^{-1} in all the samples was related to the incorporation of carbonate groups in the HAp layer (thereby actually leading to the formation of HCA, in perfect agreement with EDX analysis reported in Figure 5 and/or to the structural groups of PCL [45]. Also, the C=O bands in the range of (1600-1800) and C-H bands in the range of (2800-3000) are associated with PCL structural groups.

3.6 pH measurements

The results of the pH measurement of SBF in the periods of 0, 1, 4, 6, 8, 12, and 14 days are shown in Figure 7. The pH of the solution increased during the incubation time, especially within the first day of soaking. The increase in pH values is related to the partial dissolution of the glass during the stages of the bioactivity process associated with the formation of a HAp layer on the surface of the 3D printed scaffolds, which in line with previous studies [46–48].

Figure 7: The results of pH measurements of SBF containing 3D printed composite scaffolds

3.7 Weight measurements

The results of weight measurements of the SBF-incubated scaffolds in the periods of 0, 1, and 14 days are shown in Table 4. The weight of the scaffolds was shown to increase during the incubation time, which might be related to the formation of the HAp layer on the surface of the samples; this is consistent with the results of previously-reported investigations on SBF-incubated scaffolds [49]. Moreover,

the increased mass of the scaffolds could be the result of the water uptake by PCL, which was previously mentioned elsewhere [50].

Table 4: Results of weight measurements (%) of the 3D printed scaffold post-immersion in SBF

Sample	Increase of the weight (%)	
	1 day	14 day
PCL	0.71 ± 0.10	13.10 ± 1.10
PCL/BG-Ca	0.94 ± 0.12	19.20 ± 2.01
PCL/BG-Sr	1.50 ± 0.15	27.10 ± 3.10
PCL/BG-CaCo	1.50 ± 0.12	26.8 ± 2.26
PCL/BG-SrCo	1.40 ± 0.08	25.3 ± 1.29

3.8 Ion release profile

The concentrations of Ca^{2+}, Sr^{2+}, and Co^{2+} ions in SBF were measured by using AAS analysis after 1, 4, and 14 days (Table 5). According to Table 5, the concentration of Ca^{2+} ions generally decreased during the incubation times as a result of the formation of the HAp layer on the surface of scaffolds. This trend is consistent with the results previously reported by other authors about the behavior of some melt-derived glasses, such as 13-93 [26] and MBGs [51]. The

Table 5: Obtained data of ion release from 3D printed scaffolds in SBF, recorded by using AAS analysis

Scaffold type	Time (day)	Ca (ppm)	Sr (ppm)	Co (ppm)
PCL/BG-Ca	0	131	0	0
	1	131	0	0
	4	101	0	0
	14	80	0	0
PCL/BG-Sr	0	131	0	0
	1	131	1.7	0
	4	105	2.1	0
	14	82	3.1	0
PCL/BG-CaCo	0	131	0	0
	1	130	0	0.1
	4	112	0	0.2
	14	86	0	0.4
PCL/BG-SrCo	0	131	0	0
	1	130	3.5	0.1
	4	110	5.4	0.2
	14	84	7.4	0.5

release of Sr^{2+} and Co^{2+} ions occurred from the relevant PCL/BG-Sr, PCL/BG-CaCo, and PCL/BG-SrCo scaffolds. The higher release of Sr^{2+} and Co^{2+} ions from PCL/BG-SrCo scaffolds compared to the other batches can be attributed to the higher concentration of structural defects in these BGs and is in line with our previous study [13].
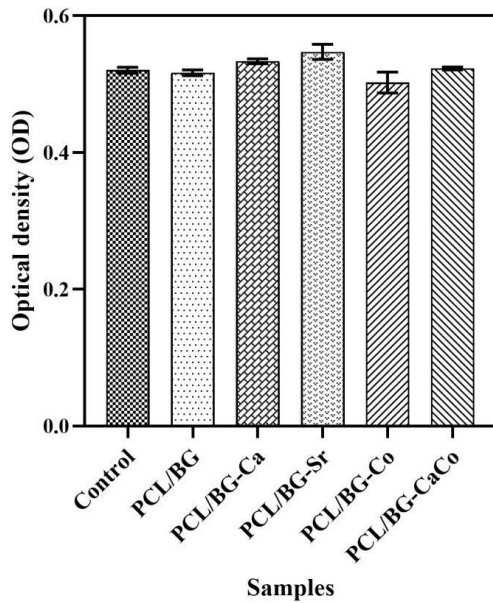

Figure 8: The viability results of MG-63 osteosarcoma cells after incubation with different 3D printed PCL/BGs scaffolds after 24 h. The statistical assessments revealed no significant differences (p < 0.05) between the control group and the experimental groups (the cells incubated with the scaffolds). Data are shown as mean values ± standard deviation (SD)

3.9 Cell viability

The results of the cytocompatibility of the prepared scaffolds are shown in Figure 8. The obtained data indicated that the scaffolds have no adverse effect on the cell growth and proliferation of MG-63 osteosarcoma cells after 24 h incubation. This result was predictable as regards the nature of the fabricated scaffolds; PCL is a non-toxic polymer with a long successful history in medicine, and BGs are also defined as safe biomaterials in the biomedical setting [52].

3.10 Cell attachment study

The FESEM images showed the expansion and attachment of MG-63 cells onto all the prepared scaffolds (see Figure 9). According to the taken micrographs, the MG-63 cells were well adhered to and expanded onto the 3D printed constructs. As shown, the incorporation of BGs into PCL could improve the attachment of the MG-63 cells onto the scaffold surface. These results were in line with previously-reported experiments stating the positive effects of BGs in improving the wettability of polymeric substrates and consequent cell attachment and expansion. It should be emphasized that the freeze-drying technique could cause adverse effects on cell-seeded constructs including the possibilities of shrinkage/drying artifacts during the process, therefore utilizing the critical point drying would be considered in future studies.
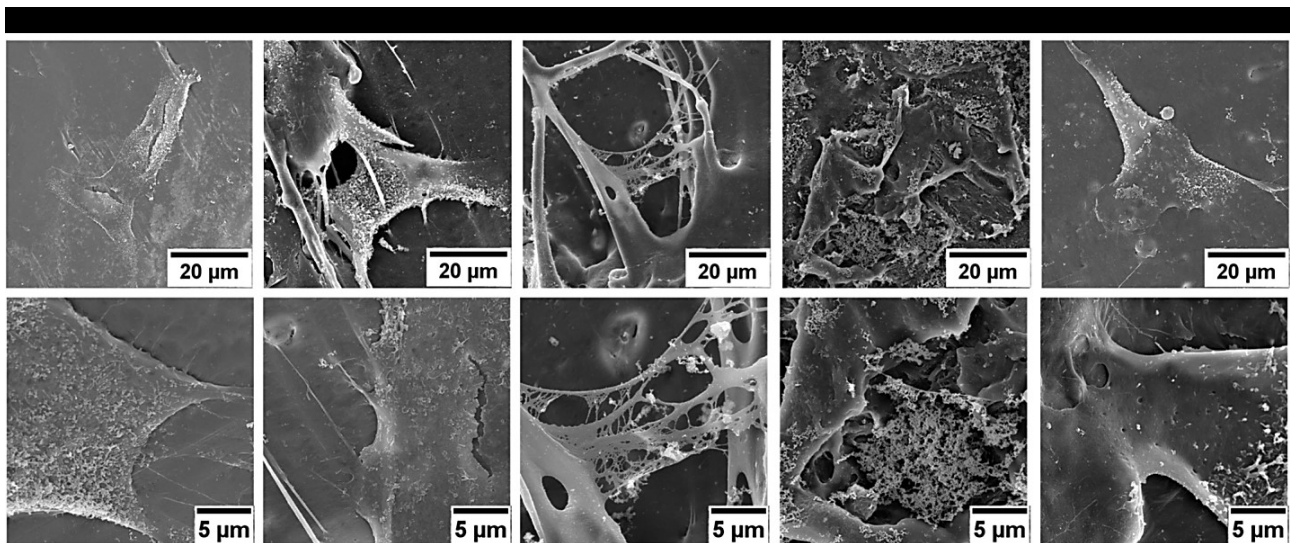
Figure 9: SEM images showing the attachment and growth of MG-63 osteosarcoma cells onto different 3D printed PCL/BGs at 3 days post-seeding

4 Conclusion

3D printed scaffolds comprising a matrix of PCL and different Sr- and/or Co-doped multi-component glasses as bioactive inclusions were successfully fabricated by using an additive manufacturing process, FDM technique. The presence of BG particles in the polymer substrate was confirmed by XRD and FESEM analyses. The fabricated composites showed improved mechanical properties based on Young's modulus results and exhibited bioactivity features regarding the apatite-forming ability to the otherwise inert PCL. *In vitro* cytotoxicity assessment and cell attachment evaluation confirmed the lack of adverse effects of the scaffolds on the growth and proliferation of osteoblastic cells. Still, further molecular assessments are needed to be able to draw a comprehensive conclusion on the effectiveness of the composites, and then performing *in vivo* functional studies on the laboratory animals may be a step forward in the concept of bone tissue regeneration.

**Conflict of Interests:** The authors declare no conflict of interest regarding the publication of this paper.

Ethical approval: The conducted research is not related to either human or animals use.

References

[1] Kargozar S., Mozafari M., Hamzehlou S., Brouki Milan P., Kim H.-W., Baino F.. Bone tissue engineering using human cells: a comprehensive review on recent trends, current prospects, and recommendations, Appl. Sci., 2019, 9 (1), 174.

[2] Qu H., Fu H., Han Z., Sun Y. 2019. Biomaterials for bone tissue engineering scaffolds: a review. RSC Adv 9 (45). 26252-26262.

[3] Neufurth M., Wang X., Wang S., Steffen R., Ackermann M., Haep N. D., *et al.* 2017. 3D printing of hybrid biomaterials for bone tissue engineering: Calcium-polyphosphate microparticles encapsulated by polycaprolactone. Acta Biomater. 64. 377-388.

[4] Dwivedi R., Kumar S., Pandey R., Mahajan A., Nandana D., Katti D. S., *et al.* 2020. Polycaprolactone as biomaterial for bone scaffolds: Review of literature. J Oral Biol Craniofac Res 10 (1). 381-388.

[5] Calciolari E., Mardas N., Dereka X., Anagnostopoulos A., Tsangaris G., Donos N. 2018. Protein expression during early stages of bone regeneration under hydrophobic and hydrophilic titanium domes. A pilot study. J. Periodontal Res. 53 (2). 174-187.

[6] Lotz E. M., Olivares-Navarrete R., Berner S., Boyan B. D., Schwartz Z. 2016. Osteogenic response of human MSCs and osteoblasts to hydrophilic and hydrophobic nanostructured titanium implant surfaces. J Biomed Mater Res A 104 (12). 3137-3148.

[7] Kermani F., Kargozar S., Tayarani-Najaran Z., Yousefi A., Beidokhti S. M., Moayed M. H. 2019. Synthesis of nano HA/βTCP mesoporous particles using a simple modification in granulation method. Mater. Sci. Eng., C 96. 859-871.

[8] Mozafari M., Banijamali S., Baino F., Kargozar S., Hill R. G. 2019. Calcium carbonate: Adored and ignored in bioactivity assessment. Acta Biomater. 91. 35-47.

[9] da Fonseca G. F., Avelino S. d. O. M., Mello D. d. C. R., do Prado R. F., Campos T. M. B., de Vasconcellos L. M. R., *et al.* 2020. Scaffolds of PCL combined to bioglass: synthesis, characterization and biological performance. J. Mater. Sci. Mater. Med. 31. 41.

[10] Kolan K., Li J., Roberts S., Semon J. A., Park J., Day D. E., *et al.* 2019. Near-field electrospinning of a polymer/bioactive glass composite to fabricate 3D biomimetic structures. International Journal of Bioprinting 5 (1).

[11] Tamjid E., Bagheri R., Vossoughi M., Simchi A. 2011. Effect of particle size on the in vitro bioactivity, hydrophilicity and mechanical properties of bioactive glass-reinforced polycaprolactone composites. Mater. Sci. Eng., C 31 (7). 1526-1533.

[12] Hoppe A., Mouriño V., Boccaccini A. R. 2013. Therapeutic inorganic ions in bioactive glasses to enhance bone formation and beyond. Biomater. Sci 1 (3). 254-256.

[13] Kermani F., Mollazadeh Beidokhti S., Baino F., Gholamzadeh-Virany Z., Mozafari M., Kargozar S. 2020. Strontium-and Cobalt-Doped Multicomponent Mesoporous Bioactive Glasses (MBGs) for Potential Use in Bone Tissue Engineering Applications. Materials 13 (6). 1348.

[14] Kargozar S., Montazerian M., Fiume E., Baino F. 2019. Multiple and promising applications of Sr-containing bioactive glasses in bone tissue engineering. Front. Bioeng. Biotechnol. 7. 161.

[15] Kargozar S., Lotfibakhshaiesh N., Ai J., Mozafari M., Brouki Milan P., Hamzehlou S., *et al.* 2017. Strontium- and cobalt-substituted bioactive glasses seeded with human umbilical cord perivascular cells to promote bone regeneration via enhanced osteogenic and angiogenic activities. Acta Biomater. 58. 502-514.

[16] Ma H., Feng C., Chang J., Wu C. 2018. 3D-printed bioceramic scaffolds: From bone tissue engineering to tumor therapy. Acta Biomater. 79. 37-59.

[17] Haleem A., Javaid M., Khan R. H., Suman R. 2020. 3D printing applications in bone tissue engineering. J Clin Orthop Trauma 11. S118-S124.

[18] Hutmacher D. W. 2000. Scaffolds in tissue engineering bone and cartilage. Biomaterials 21 (24). 2529-2543.

[19] Barbeck M., Serra T., Booms P., Stojanovic S., Najman S., Engel E., *et al.* 2017. Analysis of the in vitro degradation and the in vivo tissue response to bi-layered 3d-printed scaffolds combining pla and biphasic pla/bioglass components–guidance of the inflammatory response as basis for osteochondral regeneration. Bioact. Mater. 2 (4). 208-223.

[20] Serra T., Planell J. A., Navarro M. 2013. High-resolution PLA-based composite scaffolds via 3-D printing technology. Acta Biomater. 9 (3). 5521-5530.

[21] Kolan K. C., Semon J. A., Bindbeutel A. T., Day D. E., Leu M. C. 2020. Bioprinting with bioactive glass loaded polylactic acid composite and human adipose stem cells. Bioprinting 18. e00075.

[22] Kargozar S., Lotfibakhshaiesh N., Ai J., Samadikuchaksaraie A., Hill R. G., Shah P. A., *et al.* 2016. Synthesis, physico-chemical

and biological characterization of strontium and cobalt substituted bioactive glasses for bone tissue engineering. J. Non-Cryst. Solids 449. 133-140.

[23] Yun H.-s., Kim S.-e., Park E. K. 2011. Bioactive glass–poly (ε-caprolactone) composite scaffolds with 3 dimensionally hierarchical pore networks. Mater. Sci. Eng., C 31 (2). 198-205.

[24] Landi E., Tampieri A., Celotti G., Sprio S. 2000. Densification behaviour and mechanisms of synthetic hydroxyapatites. J. Eur. Ceram. Soc. 20 (14-15). 2377-2387.

[25] Kokubo T., Takadama H. 2006. How useful is SBF in predicting in vivo bone bioactivity? Biomaterials 27 (15). 2907-2915.

[26] Nommeots-Nomm A., Labbaf S., Devlin A., Todd N., Geng H., Solanki A. K., *et al.* 2017. Highly degradable porous melt-derived bioactive glass foam scaffolds for bone regeneration. Acta Biomater. 57. 449-461.

[27] Ghasemi-Mobarakeh L., Prabhakaran M. P., Morshed M., Nasr-Esfahani M.-H., Ramakrishna S. 2008. Electrospun poly (ε-caprolactone)/gelatin nanofibrous scaffolds for nerve tissue engineering. Biomaterials 29 (34). 4532-4539.

[28] Li X., Shi J., Dong X., Zhang L., Zeng H. 2008. A mesoporous bioactive glass/polycaprolactone composite scaffold and its bioactivity behavior. J Biomed Mater Res A 84 (1). 84-91.

[29] Ma T., MacKenzie J. D. 2019. Fully printed, high energy density flexible zinc-air batteries based on solid polymer electrolytes and a hierarchical catalyst current collector. Flex. Print. Electron. 4 (1). 015010.

[30] Thornton A., Saad J., Clayton J. 2019. Measuring the critical attributes of AM powders. Met. Powder Rep. 74 (6). 314-319.

[31] Rad R. M., Alshemary A. Z., Evis Z., Keskin D., Tezcaner A. 2020. Cellulose acetate-gelatin coated boron-bioactive glass biocomposite scaffolds for bone tissue engineering. Biomed Mater.

[32] Narayanan V., Sumathi S., Narayanasamy A. N. R. 2020. Tricomponent composite containing copper-hydroxyapatite/chitosan/polyvinyl pyrrolidone for bone tissue engineering. J Biomed Mater Res A 108 (9). 1867-1880.

[33] Baino F., Fiume E., Barberi J., Kargozar S., Marchi J., Massera J., *et al.* 2019. Processing methods for making porous bioactive glass-based scaffolds—A state-of-the-art review. Int. J. Appl. Ceram. Technol. 16 (5). 1762-1796.

[34] Kweon H., Yoo M. K., Park I. K., Kim T. H., Lee H. C., Lee H.-S., *et al.* 2003. A novel degradable polycaprolactone networks for tissue engineering. Biomaterials 24 (5). 801-808.

[35] Chen E.-C., Wu T.-M. 2007. Isothermal crystallization kinetics and thermal behavior of poly (ε-caprolactone)/multi-walled carbon nanotube composites. Polym. Degradation Stab. 92 (6). 1009-1015.

[36] Visan A. I., Popescu-Pelin G., Gherasim O., Mihailescu A., Socol M., Zgura I., *et al.* 2020. Long-term evaluation of dip-coated pcl-blend-peg coatings in simulated conditions. Polymers 12 (3). 717.

[37] An J., Teoh J. E. M., Suntornnond R., Chua C. K. 2015. Design and 3D printing of scaffolds and tissues. Engineering 1 (2). 261-268.

[38] Ishutov S., Hasiuk F. J., Harding C., Gray J. N. 2015. 3D printing sandstone porosity models. Interpretation 3 (3). SX49-SX61.

[39] Correa E., Moncada M., Zapata V. 2017. Electrical characterization of an ionic conductivity polymer electrolyte based on polycaprolactone and silver nitrate for medical applications. Mater. Lett. 205. 155-157.

[40] Poh P. S., Hutmacher D. W., Stevens M. M., Woodruff M. A. 2013. Fabrication and in vitro characterization of bioactive glass composite scaffolds for bone regeneration. Biofabrication 5 (4). 045005.

[41] Tainio J., Paakinaho K., Ahola N., Hannula M., Hyttinen J., Kellomäki M., *et al.* 2017. In vitro degradation of borosilicate bioactive glass and poly (l-lactide-co-ε-caprolactone) composite scaffolds. Materials 10 (11). 1274.

[42] Hench L. L. 1991. Bioceramics: from concept to clinic. J. Am. Ceram. Soc. 74 (7). 1487-1510.

[43] Kermani F., Mollazadeh S., Khaki J. V. 2019. A simple thermodynamics model for estimation and comparison the concentration of oxygen vacancies generated in oxide powders synthesized via the solution combustion method. Ceram. Int. 45 (10). 13496-13501.

[44] Kermani F., Gharavian A., Mollazadeh S., Kargozar S., Youssefi A., Vahdati Khaki J. 2020. Silicon-doped calcium phosphates; the critical effect of synthesis routes on the biological performance. Mater. Sci. Eng., C 111. 110828.

[45] Nazeer M. A., Yilgor E., Yilgor I. 2019. Electrospun polycaprolactone/silk fibroin nanofibrous bioactive scaffolds for tissue engineering applications. Polymer 168. 86-94.

[46] Heid S., Boccaccini A. R. 2020. Advancing bioinks for 3D bioprinting using reactive fillers: A review. Acta Biomater. 113. 1-22.

[47] Distler T., Fournier N., Grünewald A., Polley C., Seitz H., Detsch R., *et al.* 2020. Polymer-Bioactive Glass Composite Filaments for 3D Scaffold Manufacturing by Fused Deposition Modeling: Fabrication and Characterization. Front. Bioeng. Biotechnol. 8. 552.

[48] Bejarano J., Boccaccini A. R., Covarrubias C., Palza H. 2020. Effect of Cu-and Zn-Doped Bioactive Glasses on the In Vitro Bioactivity, Mechanical and Degradation Behavior of Biodegradable PDLLA Scaffolds. Materials 13 (13). 2908.

[49] Shorvazi S., Kermani F., Mollazadeh S., Kiani-Rashid A., Kargozar S., Youssefi A. 2020. Coating Ti6Al4V substrate with the triple-layer glass-ceramic compositions using sol–gel method; the critical effect of the composition of the layers on the mechanical and in vitro biological performance. J. Sol-Gel Sci. Technol. 1-11.

[50] Houaoui A., Lyyra I., Agniel R., Pauthe E., Massera J., Boissière M. 2020. Dissolution, bioactivity and osteogenic properties of composites based on polymer and silicate or borosilicate bioactive glass. Mater. Sci. Eng., C 107. 110340.

[51] López-Noriega A., Arcos D., Izquierdo-Barba I., Sakamoto Y., Terasaki O., Vallet-Regí M. 2006. Ordered mesoporous bioactive glasses for bone tissue regeneration. Chem. Mater. 18 (13). 3137-3144.

[52] Mondal D., Griffith M., Venkatraman S. S. 2016. Polycaprolactone-based biomaterials for tissue engineering and drug delivery: Current scenario and challenges. Int J Polym Mater 65 (5). 255-265.

Supplementary data
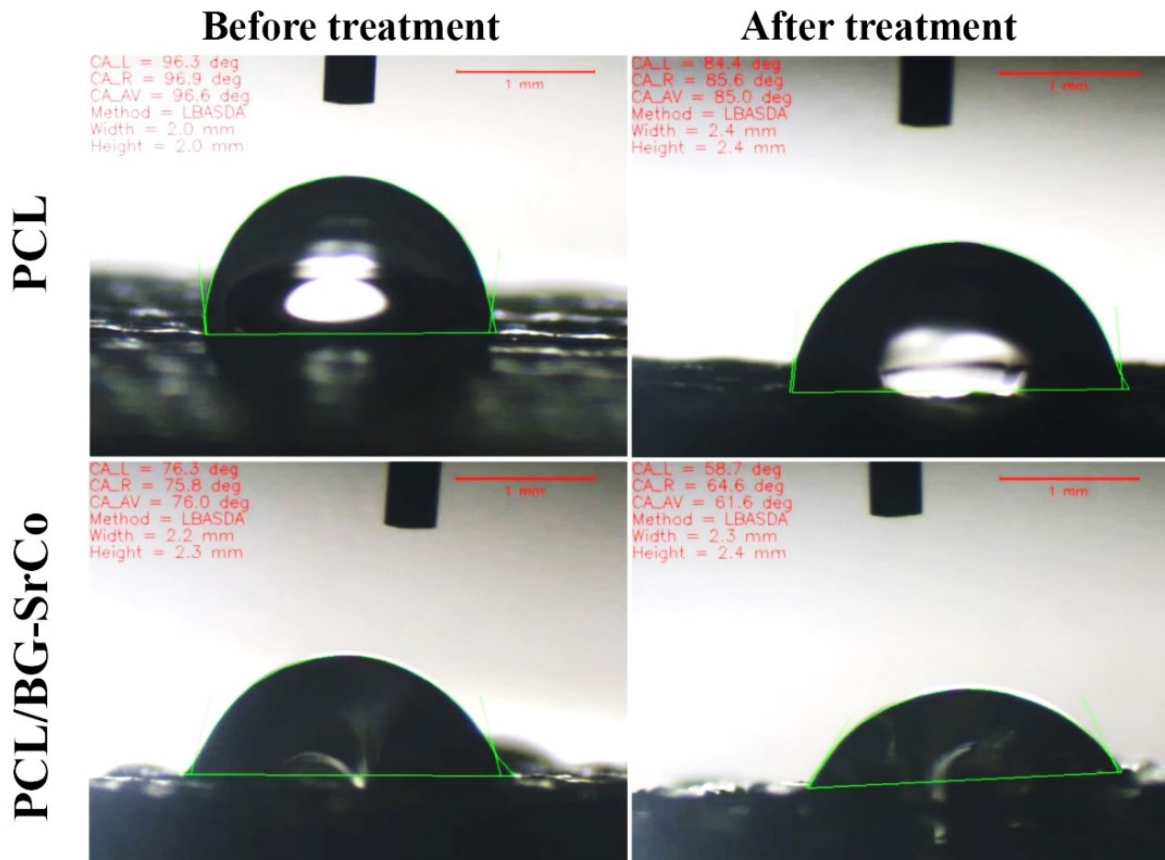
Figure S1: The surface wettability results of the prepared scaffolds before and after the surface modification with NaOH. Regarding the presented data, the average contact angle of PCL/BG-SrCo (76°) is higher than PCL (96.6°C), indicating an improvement of hydrophilicity in the scaffolds containing glass particles